1-1-2013

Impact flux on Jupiter: From superbolides to large-scale collisions

R. Hueso

S. Pérez-Hoyos

A. Sánchez-Lavega

A. Wesley

G. Hall

See next page for additional authors

A&A 560, A55 (2013)
DOI: 10.1051/0004-6361/201322216

Astronomy & Astrophysics

Impact flux on Jupiter: From superbolides to large-scale collisions

R. Hueso[1,2], S. Pérez-Hoyos[1,2], A. Sánchez-Lavega[1,2], A. Wesley[3], G. Hall[4], C. Go[5], M. Tachikawa[6], K. Aoki[6], M. Ichimaru[6], J. W. T. Pond[7], D. G. Korycansky[8], C. Palotai[7], G. Chappell[7], N. Rebeli[7], J. Harrington[7], M. Delcroix[9], M. Wong[10], I. de Pater[10], L. N. Fletcher[11], H. Hammel[12], G. S. Orton[13], I. Tabe[6], J. Watanabe[14], and J. C. Moreno[15]

[1] Física Aplicada I, Universidad del País Vasco UPV/EHU, ETS Ingeniería, Alameda Urquijo s/n, 48013 Bilbao, Spain
e-mail: ricardo.hueso@ehu.es
[2] Unidad Asociada Grupo Ciencias Planetarias UPV/EHU-IAA(CSIC), 48013 Bilbao, Spain
[3] Acquerra Pty. Ltd., 82 Merryville Drive, Murrumbateman NSW 2582, Australia
[4] Department of Physics, The University of Texas at Dallas, Richardson, Texas 75080-3021, USA
[5] Physics Department, University of San Carlos, 6000 Cebu City, Philippines
[6] Association of Lunar and Planetary Observers of Japan, 2-33-12 Misawa, Hino, 191-0032 Tokyo, Japan
[7] Planetary Sciences Group, Department of Physics, University of Central Florida, Orlando FL 32816-2385, USA
[8] Department of Earth & Planetary Sciences, University of California Santa Cruz, Santa Cruz CA 95064, USA
[9] Commission des observations planétaires, Société Astronomique de France, 2 rue de l'Ardèche, 31170 Tournefeuille, France
[10] Astronomy Department, 601 Campbell Hall, University of California, Berkeley CA 94720, USA
[11] Atmospheric, Oceanic and Planetary Physics, Clarendon Laboratory, University of Oxford, Parks Road, Oxford OX1 3PU, UK
[12] Space Science Institute, 4750 Walnut Avenue, Suite 205, Boulder CO 80301, USA
[13] Jet Propulsion Laboratory, California Institute of Technology, Pasadena CA 91109, USA
[14] National Astronomical Observatory of Japan, 2-21-1, Osawa, Mitaka, 181-8588 Tokyo, Japan
[15] Agrupación astronómica de Sabadell, 08200 Sabadell, Spain

Received 5 July 2013 / Accepted 27 September 2013

ABSTRACT

Context. Regular observations of Jupiter by a large number of amateur astronomers have resulted in the serendipitous discovery of short bright flashes in its atmosphere, which have been proposed as being caused by impacts of small objects. Three flashes were detected: one on June 3, 2010, one on August 20, 2010, and one on September 10, 2012.
Aims. We show that the flashes are caused by impacting objects that we characterize in terms of their size, and we study the flux of small impacts on Jupiter.
Methods. We measured the light curves of these atmospheric airbursts to extract their luminous energy and computed the masses and sizes of the objects. We ran simulations of impacts and compared them with the light curves. We analyzed the statistical significance of these events in the large pool of Jupiter observations.
Results. All three objects are in the 5−20 m size category depending on their density, and they released energy comparable to the recent Chelyabinsk airburst. Model simulations approximately agree with the interpretation of the limited observations. Biases in observations of Jupiter suggest a rate of 12−60 similar impacts per year and we provide software tools for amateurs to examine the faint signature of impacts in their data to increase the number of detected collisions.
Conclusions. The impact rate agrees with dynamical models of comets. More massive objects (a few 100 m) should impact with Jupiter every few years leaving atmospheric dark debris features that could be detectable about once per decade.

Key words. meteorites, meteors, meteoroids – planets and satellites: atmospheres – planets and satellites: individual: Jupiter

1. Introduction

The solar system contains large populations of minor bodies in orbits that permit collisions with the planets. Direct observation of such collisions outside the Earth has only been possible a few times. These observations include small impacts on the Moon, Mars, Venus, and Jupiter. Meteoritic impacts on the Moon have been observed from ground-based observations as light flashes on its night side (Ortiz et al. 2000). Since the Moon is so close to Earth, observing lunar impacts has direct implications for impact rate estimates for our planet (Ortiz et al. 2006). A meteoroid entering the atmosphere of Mars was observed by the Spirit Rover (Bell et al. 2004; Selsis et al. 2005), and the Pioneer Venus mission could have spotted the tail of an atmosphere-grazing meteor (Huestis & Slanger 1993) in data gathered by the Ultraviolet Spectrometer in 1979. Additionally, craters formed on Mars during the observations of the Mars Global Surveyor (Malin et al. 2006; Byrne et al. 2009) and Mars Reconnaissance Orbiter (Daubar et al. 2013) provide partial information on the present-day impact cratering rate on Mars. Recently, ejecta clouds in Saturn's rings observed by the *Cassini* spacecraft close to equinox have been linked to impacts with meteoroids of 20 cm to 1 m in diameter (Tiscareno et al. 2013), thereby providing estimates of meteoroids collisions in the outer solar system.

The giant planet Jupiter offers a much larger cross section and gravitational attraction than the inner planets and at least six collisions have been observed on the planet. Voyager 1 photographed the entry of a small meteor in Jupiter's atmosphere in a long-exposure image of the planet's night side with an estimated mass of 11 kg (Cook & Duxbury 1981). In 1994 the fragmented Shoemaker-Levy 9 (SL9) comet impacted the planet in a

series of collisions that were observed from the ground and from the *Galileo* Orbiter during its cruise to Jupiter (Noll et al. 1996; Harrington et al. 2004). In July 2009, Jupiter was impacted either by a 500−1000 m icy or by a 200−500 m rocky object that left a large-scale debris feature observable over months from ground-based observations and was discovered only hours after the impact by Anthony Wesley, an amateur astronomer (see report by Sánchez-Lavega et al. 2010).

The nature of this object is being debated because spectral signatures showed hints of a possible asteroidal origin (Fletcher et al. 2010; Orton et al. 2011). Although smaller than the SL9 comet, this impact hinted at a higher than expected impact rate on Jupiter. Small impacts of 10 m-class objects have also been detected by the short one- to two-second fireballs produced as these objects enter the atmosphere of the planet releasing large amounts of energy (Hueso et al. 2010b). Three of these Jovian superbolides have been found in video observations obtained by amateur astronomers on June 3, 2010, August 20, 2010, and September 10, 2012 during times when Jupiter was relatively close to opposition and many amateurs were observing the planet. Other plausible but unconfirmed collisions with Jupiter have been proposed, such as a dark spot on Jupiter observed by Cassini in 1690 with morphological characteristics and behavior similar to SL9 debris features (Tabe et al. 1997) and suggested as being caused by an impact with a 600 m object (Zahnle et al. 2003).

Observing collisions with Jupiter is interesting for several reasons. First, impacts such as the SL9 and the 2009 impacts, allow us to directly study the consequences of a large impact in a planetary atmosphere (Hammel et al. 2010; de Pater et al. 2010; Sánchez-Lavega et al. 2011; Pérez-Hoyos et al. 2012; Fletcher et al. 2010, 2011; Baines et al. 2013). Second, small objects producing bolides give us insight into the physics of atmospheric impacts at much higher velocities (~60 km s^{-1}) than in similar objects colliding with the Earth (11−20 km s^{-1}). Third, small impacts on Jupiter may constrain the impact rate on this planet and therefore help to constrain the small-body population in the outer solar system. Additionally, large impacts modify the atmospheric composition of the planet at the stratosphere (Cavalié et al. 2013) but the overall role of large and small impacts hitting Jupiter over time still needs to be determined. Finally, an unanswered key question is whether the presence of a giant planet like Jupiter constitutes a defense against impacts in the inner solar system or if, on the contrary, its presence perturbs enough orbits of small objects to increase the chances of collisions with the inner planets. The idea of Jupiter as a protector (Wetherill 1994) comes from the facts that the mass of the planet is enough to expel comets that might hit Earth out of the solar system and that it would attract dangerous asteroids and other objects, thereby making Earth a more secure home. Nevertheless, the overall role of Jupiter is complex with different outcomes for different populations of small solar system objects, which seriously questions the role of Jupiter as a shield (Horner & Jones 2008, 2009; Horner et al. 2010; Horner & Jones 2012).

In this paper we focus on small-size objects impacting Jupiter and producing light flashes observable from Earth. The outline of this paper is as follows. In Sect. 2 we describe the amateur observations of the three bolides that have been detected in Jupiter. In Sect. 3 we present detailed observations performed with professional equipment to search for atmospheric debris after each of these collisions. In Sect. 4 we analyze these observations, estimate the mass of the objects, and revise our previous values for the June 2010 impact (Hueso et al. 2010b). In Sect. 5 we describe numerical simulations of the effect these small objects may have on the Jovian atmosphere. In Sect. 6 we present an estimation of the current rate of impacts on Jupiter. In Sect. 7 we discuss observations and software tools able to detect impacts with Jupiter. We summarize our conclusions in Sect. 8.

2. Amateur detections of bolides in Jupiter

2.1. June 3, 2010

On June 3, 2010 at approximately 20:31:20 UT Anthony Wesley (A.W., Murrumbateman, Australia) detected a bright flash in his video recording of Jupiter using a 37 cm diameter telescope. The same event was captured by Christopher Go (C.G., Cebu, Philippines), who used a 28 cm telescope. This flash has been analyzed in detail by Hueso et al. (2010b), and here we review our previous analysis and put this object into context with the later bolides. Because the flash was detected simultaneously from two different geographical locations, it unambiguously occurred in Jupiter and not in Earth's atmosphere. The flash occurred close to Jupiter's limb in the equatorial region, at longitude 159°W (system III) and planetographic latitude 16.5°S. The flash was only visible for a few seconds and did not leave any visible trace or impact debris in observations acquired seconds later. The video observations operated at a rate of 60 (A.W.) and 55 (C.G.) frames per second (fps). Both observers used a monochrome Point Grey Flea3 camera equipped with the ICX618ALA chip. A.W. was using a red filter from Astrodon, and C.G. was using a blue filter from Edmund Scientific with effective wavelengths of 650 and 435 nm, respectively.

The first two rows in Fig. 1 display frames of these observations one second before the flash, at the brightest moment of the flash and one second later. Although the flash is clearly detected, it is short enough to be difficult to identify in a long observing session. A.W. realized the presence of the bright flash on his computer screen, and C.G. found the flash later in his observations following an alert issued by A.W. The size of the bright spot is determined by the telescope diffraction limit at the given wavelengths (0.44″ in the observation by A.W. and 0.40″ in the observation by C.G.) and atmospheric seeing. These diffraction limits correspond to about four pixels in both detectors. However, the atmospheric seeing distorts the signal from a point source into a circularly blurred spot of approximately 11 pix in diameter, which is in both cases consistent with an estimated seeing of about 1.0″.

2.2. August 20, 2010

On August 20, 2010 a second flash on Jupiter was detected by Japanese amateur astronomers. Masayuki Tachikawa (M.T., Kumamoto city) recorded a light flash at 18:21:56 UT. The flash location was roughly at planetographic latitude 21.5° north and 337° longitude (system III) in Jupiter's north equatorial belt. Kazuo Aoki (K.A., Tokyo) and Masayuki Ichimaru (M.I., Toyama city) obtained recordings of the event from locations separated about 800 km from Kumamoto, confirming the Jovian origin for the flash (Watanabe et al. 2012). A fourth observer, Takanori Wakamatsu of Arita City, found the impact in his data a few months later but with a lower signal-to-noise ratio, and his video is not analyzed in this work. The telescopes used were refractors with apertures of 15 cm (M.T.), 23.5 cm (K.A.), and 12.5 cm (M.I.). The cameras were Philips ToUcam Pro II attached to the telescope (M.T. and K.A.) providing RGB images of the planet and operated at 30 and 15 fps, respectively. M.I. recorded a 30 fps movie from a projection through a 7 mm

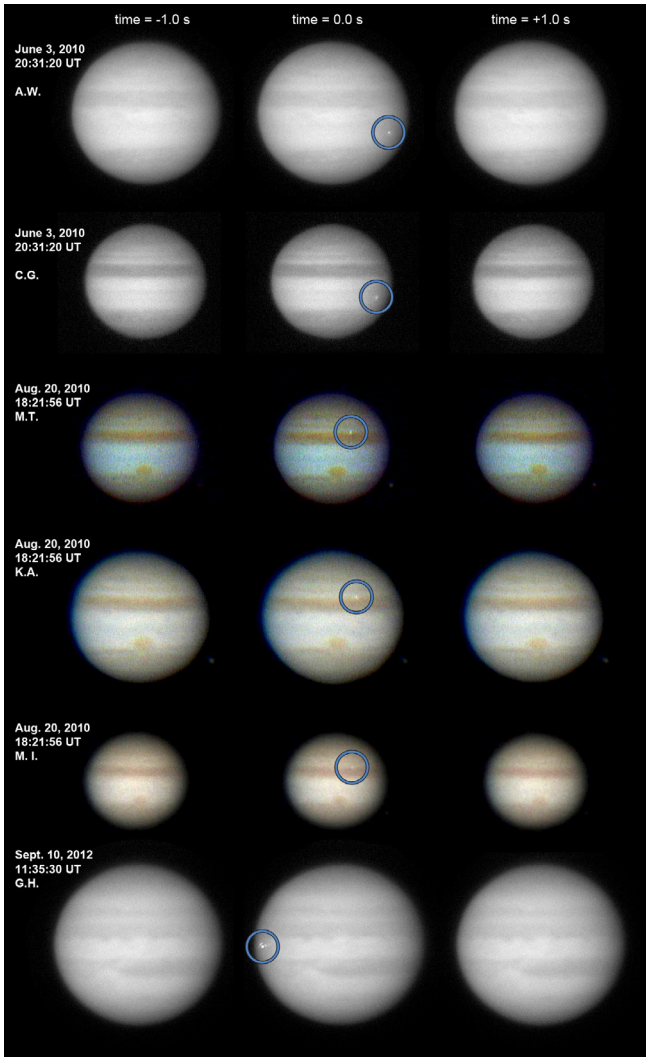

Fig. 1. Images showing the six recordings of three Jovian bolides. Differences in sizes are caused by differences in the original data and depend on the specifics of the telescope and camera used. The central column corresponds to the brightest frame where each impact is visible (circles). The left and right columns correspond to frames recorded one second before and after the impact brightest frame. The impact is still barely visible in the right column for the A.W. and G.H. recordings obtained with the largest aperture telescopes.

eyepiece. The image quality in each of the recordings was lower than in the previous impact, and the contrast of the flash with the surrounding atmosphere was also lower (see Fig. 1, rows 3 to 5). The ToUcam Pro camera consists of an ICX098BQ CCD detector covered by a Bayer mask to produce RGB color images. The Bayer mask reduces the spatial resolution by a factor of 2, and strong compression artifacts are evident in individual frames, although they are less severe in the 15 fps recording by K.A. The impact flash has a size of 11−13 pixels in diameter in these videos, which is larger than the expected size from diffraction-limited images or atmospheric seeing. This was caused by digital compression artifacts in each frame with characteristic sizes of 8×8 pixels.

2.3. September 10, 2012

On September 10, 2012, Dan Petersen (D.P., Racine, Wisconsin, USA) visually spotted a bright two-second flare at 11:35:30 UT along Jupiter's eastern limb. He estimated the visual magnitude of the flash as +6.0 (comparable to the Galilean satellite Europa with visual magnitude +5.7). D.P. reported the event to the Association of Lunar and Planetary Observers, who distributed a public alert. Hours later, George Hall (G.H., Dallas, Texas, USA) realized that he had captured the flash with his 30.5 cm aperture refractor using a Point Grey Flea 3 CCD video camera while using an Astronomik Type 2c red filter. The video was obtained at 15 fps with exposure times of 35 ms. Analysis of the impact images shows that it was located at 0.7° planetographic latitude and 265° longitude (system III). The two observers were separated by 1300 km, so ruling out a non-Jovian source for the flash. The video quality was very good, and the flash itself was particularly bright when compared with previous cases (Fig. 1), with some of the frames containing a few saturated pixels at the peak of the bolide flash and showing the first diffraction ring around the central spot. The diffraction ring extends over a circular area of 15 pixels in diameter. The pixel scale in the recording is 0.107″ (or 380 km at the subsolar point), and the diffraction limit of the telescope at 640 nm was 0.52″. The flash image has a comparable size in individual and stacked frames, which shows that diffraction-limited images were obtained. The atmospheric seeing as measured from the video recording was on the order of 0.7″.

2.4. Common characteristics

In all cases the impact was detected at least by two different observers with only one of them noticing the impact and others finding the short flash in their video observations after knowing that something had hit Jupiter. This is because amateur observers stack their video observations in single images with high signal-to-noise ratios. A short-lived event is averaged with the rest of the frames disappearing from the final image. Figure 2 displays stackings of the different videos showing how the impact is apparent when all the frames where the impact is visible are added and vanishes when the observer adds more frames in the sequence that does not contain the flash.

This opens the possibility that some of these objects could have been observed in the past without realizing their nature, and it may explain why these fireball events have not been recognized before. It also suggests that past impacts could be found in a close examination of amateur data recorded by observers.

3. Searches of atmospheric debris

In July 2009, a 500 m size impactor hit Jupiter, leading to an initially 4800 km debris field that was dark in the visible and bright in methane absorption bands (Sánchez-Lavega et al. 2010; Hammel et al. 2010). The impact occurred on the night side of the planet and was discovered by amateur astronomer Anthony Wesley a few hours after the impact. The debris had significant structure in HST observations, which changed significantly over the first weeks following the impact (Hammel et al. 2010). It was observable at visible wavelengths for a few months using small size telescopes and at near mid-infrared wavelengths with professional telescopes during a minimum of six months (Sánchez-Lavega et al. 2011; de Pater et al. 2010). Additionally, mid-infrarred observations revealed significant alterations of atmospheric properties ranging from stratospheric temperatures to ammonia or hydrocarbons content (Orton et al. 2011; Fletcher et al. 2010, 2011).

In contrast, the Jovian flash on June 3, 2010 did not leave any observable feature on Jupiter's disk that could have been seen by

Table 1. Detected Jovian bolides.

Date and time	Observers	Telescope diameter	Detector	Filter (effective λ)	Sampling rate (fps)
June 3, 2010	Anthony Wesley	37 cm	Point Grey Flea3	650 nm	60
20:31:20 UT	Christopher Go	28 cm	Point Grey Flea3	435 nm	55
Aug. 20, 2010	Masayuki Tachikawa	15 cm	Philips ToUCam II	RGB	30
18:21:56 UT	Kazuo Aoki	23.5 cm	Philips ToUCam II	RGB	15
	Masayuki Ichimaru	12.5 cm	Philips ToUCam II	RGB	30
Sept.10,2012	Dan Petersen	30.5 cm	Visual observation	–	–
11:35:30 UT	George Hall	30.5 cm	Point Grey Flea3	640 nm	15

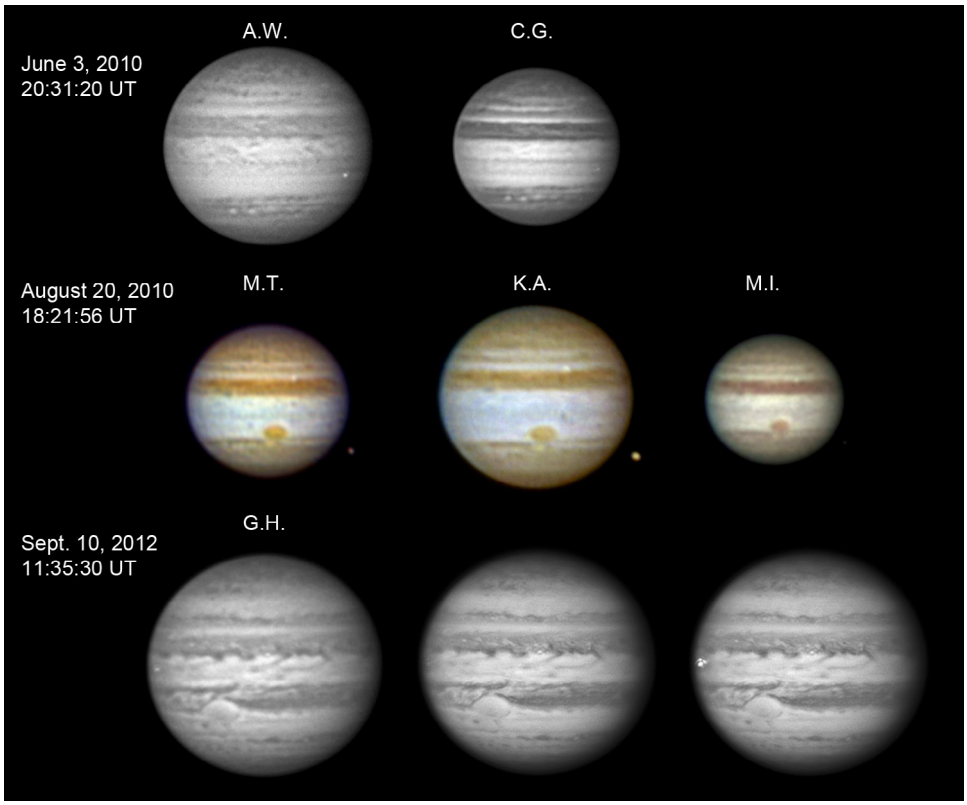

Fig. 2. Images showing the three Jovian bolides and stacking effects. Differences in sizes are due to differences in the original data and depend on the specifics of the telescope and camera used. Each image has been built by stacking enough frames to clearly show the atmosphere and the impact: 190 (A.W.), 450 (C.G.), 95 (M.T.), 40 (K.A.), 97 (M.I.), 160 (G.H. left frame), and 1000 (G.H. central frame). All images have been processed using high-pass filters to increase the contrast of atmospheric features. The higher the number of frames, the better the image quality, but the lower the contribution from the impact, which disappears after stacking of 600 frames in the high-quality observations of A.W., C.G., and G.H. This effect is noticeable in the third row of images showing three versions of the September 2012 impact. The left image is a stacking of 160 frames. The middle image is a stacking of 1000 frames including the impact. The right image shows the stacking of 1000 frames with the impact flash added as built from 20 frames. In all cases the flashes extend over several pixels because they are affected by diffraction and atmospheric seeing.

amateurs minutes after the impact or several planetary rotations later. This suggests a much smaller size for the impacting body.

The first 2010 fireball ignited visible and infrared observations on large telescopes (Keck, IRTF, and Gemini North 19 h after the impact; Gemini South and VLT 38 hours after the impact; HST 77 h after the impact, see Hueso et al. 2010b) aimed to detect any possible atmospheric debris. Figure 3 shows images of the impact area from those observations. The second flash was followed by high-quality observations from many amateur astronomers over the next few Jupiter rotations. Notable observations that could have detected a large debris field if it had been produced were acquired on August 21 by J.-J. Poupeau (03:23 UT), C. Pellier (03:25 UT), J.A. Soldevilla (03:50 UT), M. Delcroix (03:25–04:23 UT), and G. Arrillaga (04:16 UT). There were no attempts to observe this region later on with ground-based large telescopes, except for a fortuitously scheduled observing night on the Keck II telescope that was reported by de Pater et al. (2011). The third flash was followed by observations acquired two Jupiter rotations later with the NASA IRTF telescope at near infrared wavelengths where a possible debris cloud should have had a high contrast, but the image showed no distinctive features. Additionally, detailed observations were obtained ten hours after the impact by G. Walker (from 09:01 UT to 09:31 UT), J. Willingham (09:11 UT), G. Chester (09:34 UT), and W. Jaeschke (09:52 UT) with no debris observed.

All amateur images detailed in this section are publicly available on the PVOL database `http://www.pvol.ehu.es` (Hueso et al. 2010a).

Table 2. High-resolution observations of impact locations.

Telescope/instrument	Time (UT)	Hours after impact	Wavelength (λ)	Sensitivity
Keck/NIRC2	2010-06-04 15:00	+18.5	Near IR: 1.29, 1.58, 2.06, 2.12, 2.13, 2.17	A, C
IRTF/TEXES	2010-06-04 15:00	+18.5	Mid IR: 10.34, 10.74	T, N
Gemini N/NIRI	2010-06-04 15:00	+18.5	Near IR: 1.69, 2.11, 2.17	A, C
Gemini S/T-ReCS	2010-06-05 10:30	+38.0	Mid IR: 7.9, 8.8, 10.4, 18.3	T, N, A
ESO-VLT/VISIR	2010-06-05 10:30	+38.0	Mid IR: 7.9, 8.7, 10.7, 13.04, 17.54, 18.65, 19.50	T, N, A
HST/WFC3	2010-06-07 10:30	+77.5	UV: 0.225, 0.275, 0.343	A
			Visible: 0.395, 0.502, 0.631	C
			Near IR: 0.889, 0.953	A, C
Keck/NIRC2	2010-08-21 13:40	+19.2	Near IR: 1.29, 1.58, 1.65, 2.11, 2.27	A, C
IRTF	2012-09-11 19:12	+31.6	Near IR: 2.12	A

Notes. (C) clouds; (A) aerosols; (T) temperature field; (N) NH3 and other chemistry modifications. UT times show the approximate time for the central meridian crossing of the impact longitude. Observations were scheduled in a short time range around those times.

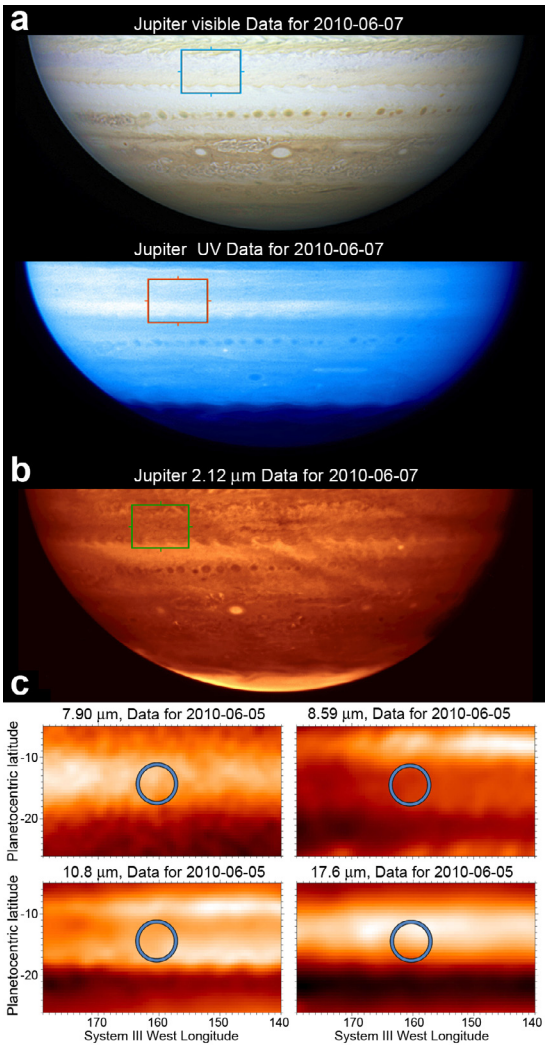

Fig. 3. Observations of the 2010 June 3 impact location. **a)** HST visible and ultraviolet (225 nm); **b)** Gemini N/NIRI in a strong methane absorption band (2.12 μm); **c)** VLT/VISIR images at (i) 7.9; (ii) 8.6; (iii) 10.8; and (iv) 17.6 μm sensitive to (i) stratospheric temperatures; (ii) aerosols; (iii) stratospheric ammonia or silicates emissions, and (iv) tropospheric structure, respectively. Debris from an impactor should appear dark in visible and ultraviolet and bright in methane absorption bands and thermal emissions. Boxes and circles show the expected debris location. Neither of these observations succeeded in showing a debris field at the impact's location, thus implying a modest size for the object.

Neither of these impacts left any detectable feature in the Jovian atmosphere across the broad spectral range from the ensemble of observations. This contrasted with expectations from the experience gathered in visible and infrared observations of SL9 (Harrington et al. 2004) and 2009 (Hammel et al. 2010; Orton et al. 2011; Fletcher et al. 2010, 2011) impacts that produced extense debris fields of aerosols, as well as alterations in NH3 content and the thermal field observable in the mid-infrared (see for instance Fig. 2 in Orton et al. (2011)). Table 2 presents a summary of the high-resolution observations performed with top-class observatories after the 2010 and 2012 impacts (Figs. 3 and 4), along with a summary of the sensitivity of each observation to different atmospheric properties. The smallest fragment of comet SL9 impacting Jupiter and leaving a briefly visible debris in HST observations was fragment N, which had an estimated size of 50 m in diameter and a density of 0.25 g/cm3 (Crawford 1997), as deduced from light curves of the fireball it produced in Jupiter's atmosphere. The debris cloud had low contrast in HST observations and either disappeared or quickly mixed with debris from other fragments. A minimum size of 200 m (from comparison with SL9 fragment D) is probably more representative of impacts leaving debris features over several Jovian rotations that are detectable at the spatial resolution achievable with HST observations (Hammel et al. 1995).

4. Analysis of video observations

4.1. Photometry

Raw light curves were obtained on difference images that enhance the visibility of the impact by subtracting a reference image from each individual frame. The reference image was obtained by coregistering and stacking a significant number of frames of the video sequence corresponding to instants before the impact normalized by the number of frames used. The difference images are dominated by single-pixel noise on the planetary limb, which is easy to remove with a simple threshold mask. The reference image and difference images were obtained using software developed in IDL based on a simplified version of our lucky imaging software tool (Sánchez-Lavega et al. 2012). The software locates the impact position automatically from the location of the most intense signal in the differential photometry and extracts photometric light curves over a circular region with a radius large enough to encompass the total light emitted by the impact. Figure 5 summarizes the procedure. Raw light curves obtained by the software are shown in Fig. 6.

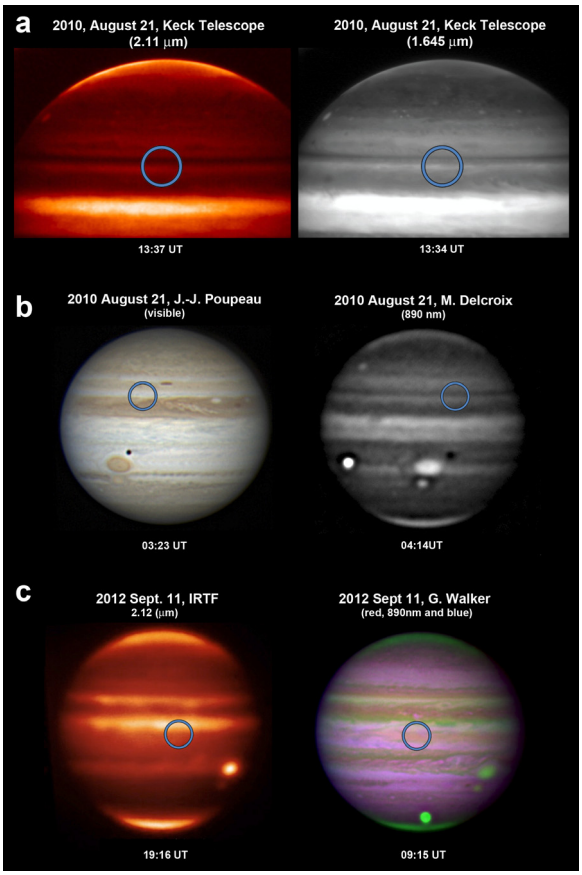

Fig. 4. Observations of the 2010 August and 2012 September impact locations. **a)** Keck images following the 2010 August 20 impact. The first image was acquired in a strong methane absorption band (2.11 μm) while the second was acquired in a narrow Fe band (1.645 μm). **b)** Amateur observations in the visible and the strong methane absorption band at 890 nm one Jupiter rotation after the impact. **c)** IRTF and amateur images obtained following the 2012 September 10 impact. Debris from an impactor should appear dark at visible wavelengths and bright in methane absorption bands in 890 nm and 2.12 μm as well as in 1.645 μm. Circles show the impact location. Neither of these observations succeeded in showing a debris field at the impacts' locations, implying modest sizes for both objects.

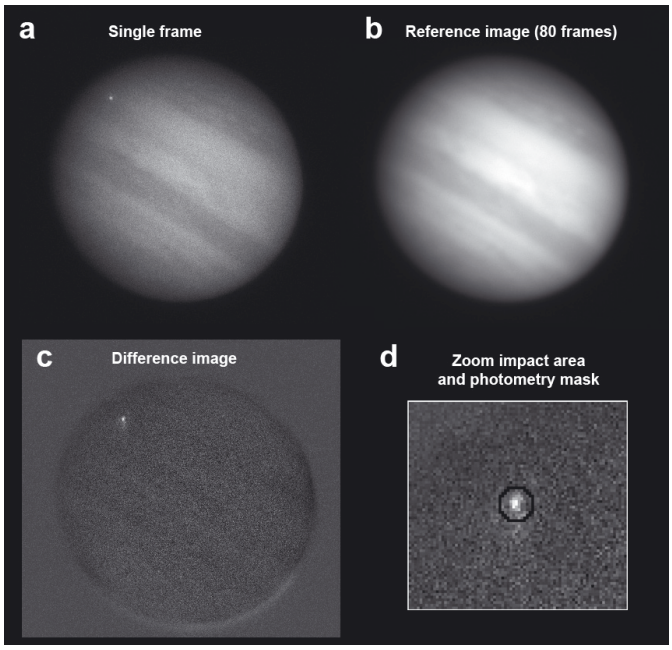

Fig. 5. Automatic analysis of impact flashes for the bolide detection by A.W. on June 3, 2010. **a)** Single frame showing the impact at its highest brightness. **b)** Reference image from coregistering and stacking 80 frames without the flash. **c)** Difference image dominated by the impact. **d)** Zoom over the impact area showing the circular mask used to extract the photometric signal of the impact.

4.2. Integrated light curves

The 2010 June 3 flash was observable for 1.9 s in red light (A.W.), and it had a first phase of slight luminosity lasting 0.15 s, a clear central peak of 1.15 s, and a distinct smaller second peak of 0.6 s. In blue light (C.G.) the flash was slightly different with a sudden disappearance flashing in total for only 0.95 s without the extended light curve observed in red light. Differences between both light curves may come from the smallest diameter of the telescope used in the blue filtered images.

The 2010 August 20 impact had a duration of 1.4 s in the video by M.T., 1.9 s in the higher quality video by K. A and 1.1 s in the noisier video by M. I. The temporal extent of the flash correlates with the size of the telescope used for the recording.

The 2012 September 10 flash was clearly observable for 1.7 s. The central part of the light curve contained five frames with saturated pixels. For those frames, the radial brightness distribution of the flash was fit to a 2D Gaussian to approximate the core of the point spread function (PSF). Based on the unsaturated data, the standard deviation of the Gaussian was set to 1.5 pixels, and only unsaturated data within five pixels of the impact site were used in the fit. Each saturated pixel in the images was replaced with the value predicted at that position by the fit. After saturation correction, the total DNs from the flash were very similar and only increased by 6% in the most saturated frame since most of the light distributes across the extended PSF, and saturated pixels are only a minor fraction of the total pixels affected by the flash. However, the double central-peak observable in the raw light curve might be an artifact of the acquisition. The fireball was still observable with very low luminosity for an extra 1.0 s in the difference images. The full light curve can be interpreted as an initial onset, followed by an explosion and a cooling down of the meteoroid trail still emitting detectable light for another second.

We integrated the total DNs corresponding to each raw light curve by adding the values appearing in Fig. 6 during the temporal duration of each flash. Photometric uncertainties for each data point were estimated from the irregularities of the light curve in frames without the impact. The photometric uncertainty for the integrated brightness was assumed as the individual uncertainty in each frame multiplied by the square root of the number of frames added.

4.3. Calibration

The calibration of the raw light curves to physical units was done by comparing the signal of the flash to the total signal of the planet using standard calibration procedures for planets. From the total solar flux arriving and reflected by Jupiter, only a portion of the energy is detected in each filtered observation. We calculated an effective wavelength $\lambda_{\rm eff}$ representative of each observation and defined as

$$\lambda_{\rm eff} = \frac{\int_{\lambda_1}^{\lambda_2} \lambda T(\lambda) {\rm d}\lambda}{\int_{\lambda_1}^{\lambda_2} T(\lambda) {\rm d}\lambda}, \quad (1)$$

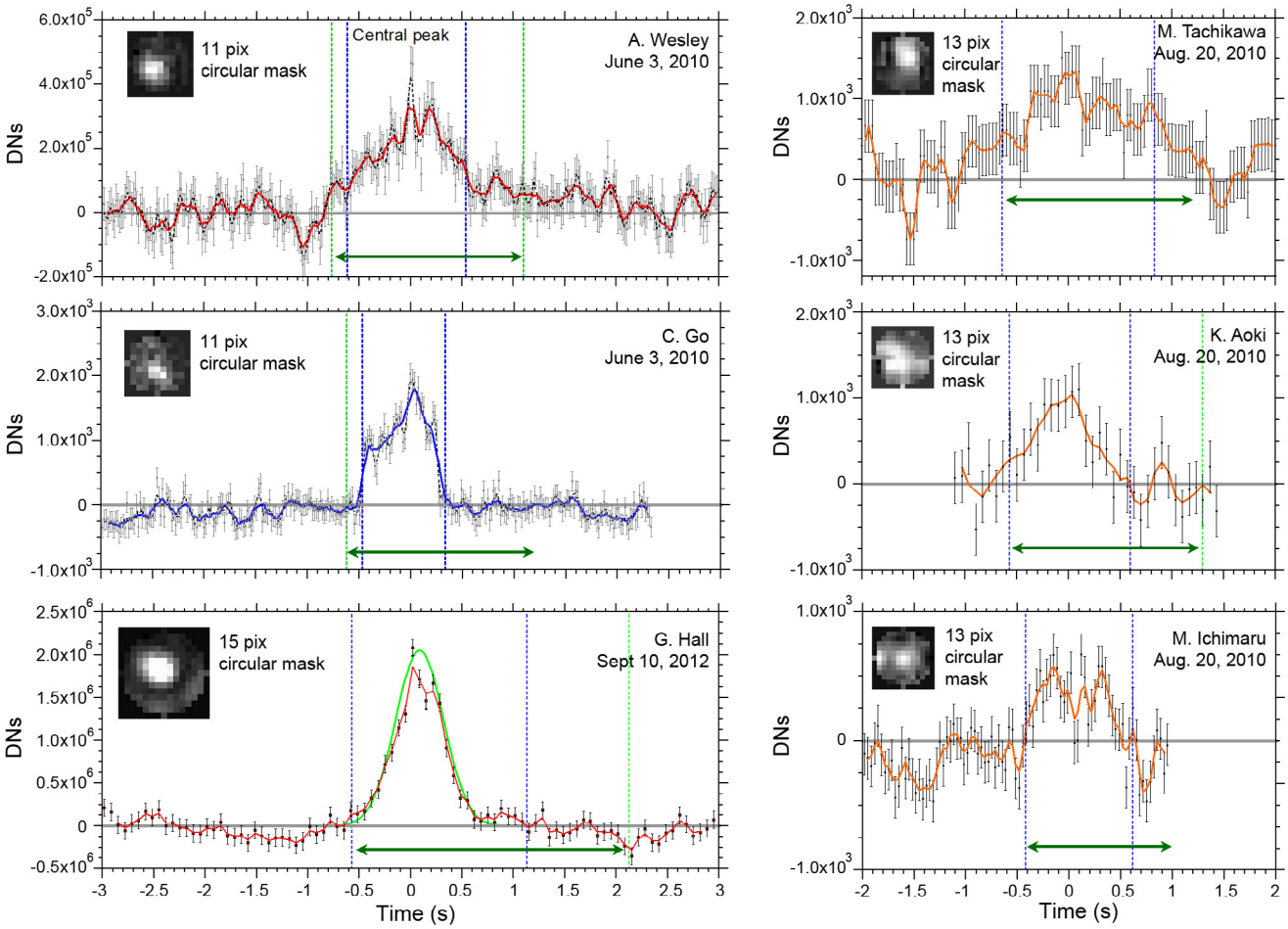

Fig. 6. Raw light curves and flash duration. Data points show the individual measurement for each frame. Error bars come from the pixel noise in the short-time exposures and small errors in the stacking procedure. They are estimated by examining the oscillations of the light curve when there is no flash in the image. Color curves represent fits to the data with running averages of 5 points. Vertical dotted blue lines represent the central flash where the structure of the flash is discernible in each individual frame. Vertical dotted green lines mark times when the flash is difficult to identify in individual frames but is observable in the difference images. *Insets* show the circular box of pixels used to extract the differential photometry and the flash in the brightest frame. G. Hall's light curve displays a Gaussian fit shown in green. Photometric values obtained without correcting the partial saturation at the center of the impact are represented with triangles; corrected values are displayed with circles and were used for the fit. Horizontal dark-green arrows show the interval of time used to integrate the light curve in each case and are consistent with the longest duration of the flash when several observations are available. Order of magnitude differences in the digital number (DN) values come from differences in codification of brightness values in different videos.

where $T(\lambda)$ is the transmissivity of the system at each wavelength obtained by multiplying the filter and camera responses. The full-disk albedo of the Jovian disk is known for each different wavelength A_λ (Chanover et al. 1996; Karkoschka 1998; Hammel et al. 2010) and, in particular, for the effective wavelengths representative of each observation (see Fig. 7).

We also computed the "effective solar constant" at Jupiter's distance, $S_{J\mathrm{eff}}$, by scaling the solar constant at Earth, $S_\mathrm{E} = 1361 W/m^2$, to Jupiter's distance, d_J, expressed in astronomical units, and multiplying that number by the convolution of the camera and filter responses $S_\mathrm{r}(\lambda)$ with a black-body emission at $T = 5780$ K:

$$S_{J\mathrm{eff}} = \frac{S_\mathrm{E}}{{d_\mathrm{J}}^2} \frac{\int_{\lambda_1}^{\lambda_2} S_r(\lambda) B(\lambda) \mathrm{d}\lambda}{\int_0^\infty B(\lambda) \mathrm{d}\lambda}. \quad (2)$$

In the filtered observations by A.W., C. G., and G. H., we used the camera response and filter curves as supplied by the manufacturers of each piece of equipment (see Fig. 7). In the unfiltered RGB video observations of the August 2010 impact, we simply considered that 50% of the solar energy arrives in the visible part of the spectrum and that the effective full-disk albedo of the planet is an average between the blue and red albedos. We then computed the total energy reflected by Jupiter convolved with the system response as

$$E_\mathrm{J} = A_\mathrm{eff} S_{J\mathrm{eff}} \pi R_\mathrm{eq} R_\mathrm{pl}, \quad (3)$$

where A_eff is the effective albedo of the planet, and $R_\mathrm{eq} = 71\,492$ km and $R_\mathrm{pl} = 66\,854$ km are the equatorial and polar radii. Then, E_J is given in Watts and corresponds to the total DNs over the disk of the planet. Dividing E_J by the total DNs of Jupiter, we obtain a conversion factor that allows transforming DNs to Watts. A conversion to Joules is immediate by multiplying this factor by the time represented by each frame. The total luminosity of each flash is found by adding the total DNs excess for each flash, and they are computed from the raw light curves in Fig. 6 following the temporal duration of the flash. Results are summarized in Table 3 where conversion factors from DNs to Joules, as well as intermediate steps in the calibration, are given.

Table 3. Impact energies.

Observer	Effective solar constant	Full-disk albedo	Jupiter reflected power (W)	Jupiter DNs	Flash DNs	1*DN* (J)	Flash energy (J)
A.W.	6.6 W/m^2	0.50	4.96×10^{16}	2.51×10^9	$(18.1 \pm 0.8) \times 10^6$	3.29×10^5	$(6.0 \pm 0.3) \times 10^{12}$
C.G.	6.2 W/m^2	0.40	5.30×10^{16}	5.92×10^6	$(4.9 \pm 0.1) \times 10^4$	1.14×10^8	$(5.6 \pm 0.2) \times 10^{12}$
M.T.	28 W/m^2	0.45	1.89×10^{17}	3.11×10^9	$(4.7 \pm 0.4) \times 10^4$	1.9×10^9	$(88 \pm 7.3) \times 10^{12}$
K.A.	28 W/m^2	0.45	1.89×10^{17}	7.40×10^6	$(9.8 \pm 1.2) \times 10^4$	1.6×10^9	$(16 \pm 2.0) \times 10^{12}$
M.I.	28 W/m^2	0.45	1.89×10^{17}	3.37×10^6	$(9.7 \pm 1.0) \times 10^3$	3.6×10^9	$(35 \pm 3.4) \times 10^{12}$
G.H.	4.8 W/m^2	0.50	3.67×10^{16}	2.16×10^9	$(17.0 \pm 0.7) \times 10^6$	1.1×10^6	$(19 \pm 0.6) \times 10^{12}$

Notes. Uncertainties in the flash DN and flash energy columns are based solely on photometric uncertainties in Fig. 6. The order-of-magnitude variations in the total Jupiter DNs for different videos come from different image codifications in the original data.

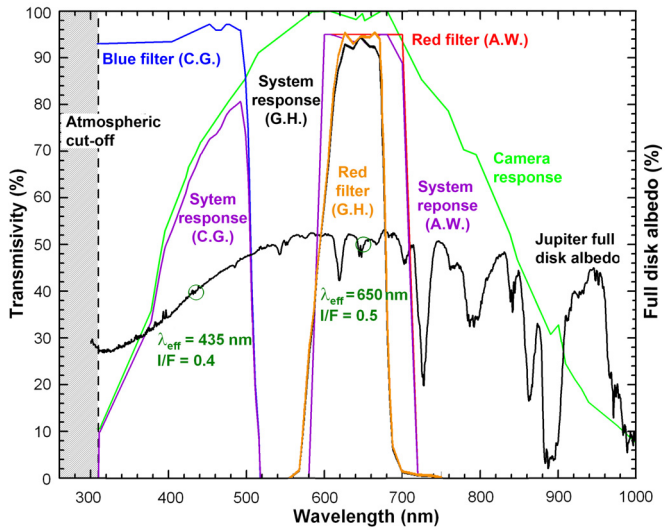

Fig. 7. Jupiter albedo and system responses for the monochromatic observations of A.W., C.G., and G.H.

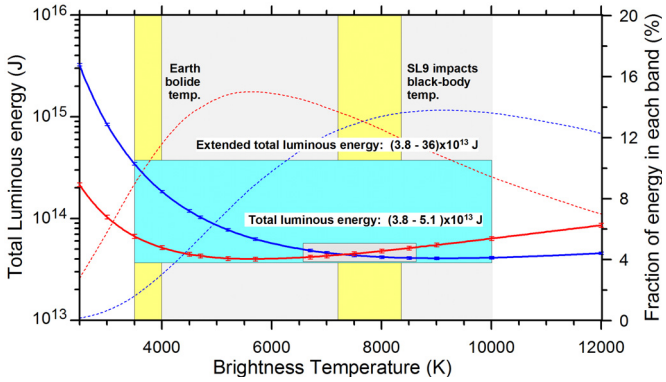

Fig. 8. Total luminous energy for the June 2010 event as a function of bolide black body temperature. Dotted lines (right axis) represent the fraction of flash energy detected in each filter observation. Red indicates the red-band images acquired by A.W. Blue indicates the blue-band images acquired by C.G. Deconvolving the detected light with these efficiencies, we obtain the total luminous energy as deduced from each video observation independently. Error bars represent uncertainties from the light curve analysis. Results from both observations agree in the gray box, indicating a range of temperatures from 6500 K to 8500 K. An extended set of temperatures is obtained from comparison with Earth bolides. The extended set of possible temperatures 3500 K to 10000 K results in larger uncertainties in luminous energy marked by the blue box.

We note that the June 2010 event was analyzed in our previous paper using a slightly different calibration procedure to the one used here (Hueso et al. 2010b). In particular there was an error in the effective solar constant that has been corrected in this work.

4.4. Luminous energies and masses

Integrated energies appearing in Table 3 represent only a fraction of the total luminous energy emitted by each fireball, and this fraction depends on the emission temperature and the camera and filter responses that must be deconvolved to obtain the total luminous energy of each flash. We assume the flash's spectral emission can be described by a black-body law. Figure 8 shows the fraction of energy emitted in the red and blue wavelength ranges of the June 2010 impact and the total luminous energy of the fireball deconvolved from the system response at each temperature. Comparing both curves, we obtain compatible results for both observations with temperatures ranging over 6500–8500 K. These temperatures encompass those derived for the optical flashes observed by the *Galileo* spacecraft in Shoemaker-Levy 9 impacts (7800 ± 600 K; Chapman 1996), and they are significantly higher than those derived for bolides entering Earth's atmosphere (3700 ± 100 K for the 2008 TC3 asteroid; Borovička & Charvát 2009). We assume that emission temperatures are not well constrained from this observation and extend the range of possible temperatures for the emission flash from 3500−10 000 K (as the upper limit fixed by numerical simulations later presented). From the behavior displayed in Fig. 8, lower temperatures (releasing most of their luminous energy in the infrared) result in greater total luminous energies (especially for the blue observations), while higher temperatures (releasing most of their energy in the visible) result in lower total luminosities. For the August 2010 and September 2012 events, we do not have comparable information to retrieve temperatures so we use the same extended range of black-body temperatures.

Luminous energies appearing in Fig. 8 assume isotropic emission. A correction factor comes from the fact that part of the flash energy comes from reflection in the Jovian clouds of the luminous energy emitted downward to the planet. We have assumed a 50% reflection of the downward total flux independently of the geometry. When this correction is taken into account, the total optical energy emitted in each flash can be constrained to values in the range $(3–27) \times 10^{13}$ J in the June 2010 impact, $(6–20) \times 10^{13}$ J in the August 2010 impact, and $(16–32) \times 10^{13}$ J in the September 2012 impact. Here uncertainties come from the combined uncertainties in the photometric measurements from the raw light curves in Fig. 4 and uncertainties in the brightness temperature.

Table 4. Jovian bolides analysis.

Date (yr-mm-dd)	Energy (J)	Energy (ktn)	Mass (Tn)	Diameter (m) (ρ = 2.0 g cm^{-3})	Diameter (m) (ρ = 0.6 g cm^{-3})	Diameter (m) (ρ = 0.25 g cm^{-3})
2010-06-03	$1.9–14 \times 10^{14}$	46–340	105–780	4.7–9.1	7.0–14	9.3–18
2010-08-20	$3.7–11 \times 10^{14}$	88–260	205–610	5.8–8.4	8.7–13	12–17
2012-09-10	$9.0–17 \times 10^{14}$	215–405	500–950	7.8–9.7	12–14	15–19

The efficiency in transforming kinetic energy into luminous energy has been derived for Earth bolides and is given by the experimental fit to observations of several bolides with different energies as (Brown et al. 2002)

$$\mu = 0.12E_0^{0.11} \quad (4)$$

where E_0 is the optical energy measured in kiloton of TNT (1 kiloton = 4.185×10^{12} J). Assuming this relation also holds true for the Jovian impacts, we obtain values of the efficiency parameter between 0.11 to 0.25, leading to total kinetic energies 5–10 times higher than the luminous values. The mass and radial size of the object can be computed by assuming the object impacted Jupiter with velocities of 60 km s^{-1} (similar to the SL9 collisions) and densities from 2.0 to 0.25 g/cm^3. When taking all error bars into account, the June and August 2010 bolides seem to have been produced by 5–18 m sized objects, while the September 2012 impact was produced by an object of 8–20 m. Results are summarized in Table 4.

The sizes for these impactors are close to the largest impactor detected in Saturn rings from ejecta clouds observed by the *Cassini* orbiter and estimated to have a radius of 1–10 m (Tiscareno et al. 2013). The energy released by collisions with these objects is well above those produced by intense superbolides (i.e., objects of 10 m size) entering Earth's atmosphere (Ceplecha et al. 1999). Energies are comparable to the recent Chelyabinsk airburst (400–600 ktn; Brown 2013). The highest possible energies released in the September 2012 collision is about ten times less energetic than current estimates of the Tunguska event (3–5 MTn; Boslough & Crawford 2008).

5. Numerical simulations of the 2012 impact

Since observations revealed only limited details of the 2010 and 2012 impact events, we turn to numerical modeling to gather physically self-consistent information about the entry and breakup of the impactor.

5.1. Model description

To simulate small-scale impacts we employ the ZEUS-MP 2 hydrodynamics code (Hayes et al. 2006) that was successfully used previously for modeling the SL9 (Korycansky et al. 2006; Palotai et al. 2011) and the 2009 impacts (Pond et al. 2012). The model includes a moving Cartesian grid with the following axes: x_1 is the "along-track coordinate" that is aligned with the impactor's initial trajectory, x_2 is parallel with the local horizontal, and x_3 is perpendicular to both of them. The one-bar pressure level is located at the origin of the x_1 axis.

The nominal case of our impact simulations includes a spherical, porous-ice impactor that has a uniform density of 0.6 g cm^{-3}. We considered a 16 m diameter impactor with a mass of 1290 Tn, which is slightly more massive than the observed impacts. Simulating smaller impacts is computationally more expensive by the restrictions in the model grid imposed by the small size of the object and its high velocity. From the SL9 sensitivity experiments Korycansky et al. (2006), we concluded that at least 16 grid cells are needed across the radius of an impactor (R16 resolution) to resolve the atmospheric instabilities that are ultimately responsible for breaking up the object. Higher resolution does not alter the breakup mode or the penetration depth of the impactor significantly. Within and in close proximity to our model impactor, we have a uniform R16 resolution grid that corresponds to a spacing of 50 cm per cell. The grid spacing then increases geometrically in each direction away from the R16 area with a factor of ~8% per grid cell. The grid for the nominal model has $200 \times 156 \times 170$ grid cell elements and a size of about $540 \times 160 \times 250$ m. We track the front of the impactor and adjust the velocity of the moving grid to keep the bulk of the impactor material within the high-resolution region.

Similarly to our previous studies, we use the Tillotson equation of state (EOS) that was derived for high-velocity impacts (Tillotson 1962; Melosh 1989). The parameters in the EOS for our ice impactor are identical to those listed in Korycansky et al. (2006). The Jovian atmosphere is modeled by a temperature-pressure profile that is adopted from Deming & Harrington (2001). The impactor is initially introduced at z = 150 km altitude (x_1 distances indicate along-track values, z values represent altitude above the 1 bar pressure level). Owing to the limited number of observational constraints on the impactor, we use SL9-like values for impact velocity and angle (entry speed of 60 km s^{-1} and impact angle of 43° from the local vertical). To ensure numerical stability the typical time step in our model is $\Delta t \sim 10^{-6}$ s, which makes these simulations computationally expensive. The model simulates the 2012 event, thus the impact takes place at 0.7° planetographic latitude, and the gravitational acceleration (including the J2 and centrifugal terms) is calculated at this location. A more thorough description of the model can be found in Korycansky et al. (2006).

5.2. Simulation results

The response of the impactor to the aerodynamic forces it encounters is similar to what is exhibited by an SL9- (Korycansky et al. 2006; Palotai et al. 2011) or a 2009-type object (Pond et al. 2012). Figure 9 shows the breakup process of the impactor. The compression of comet material in the direction of the motion begins very quickly, resulting in "pancaking" of the impactor that is consistent with previous Jupiter impact models. Hydrodynamical instabilities cause surface deformation and ablation of material from the impactor that is blown back and outwards.

At $t \sim 0.7$ s, the impactor begins to break up into smaller fragments at $x_1 \approx 163$ km, which corresponds to about the 3 hPa (3 mbar) pressure level. This event is visible on the energy deposition curve (Fig. 10) at $z \approx 120$ km altitude. After the breakup, large amounts of material fall off of the parent body. The organized shock system behind the impactor collapses quickly, allowing for a more turbulent flow and horizontal spreading

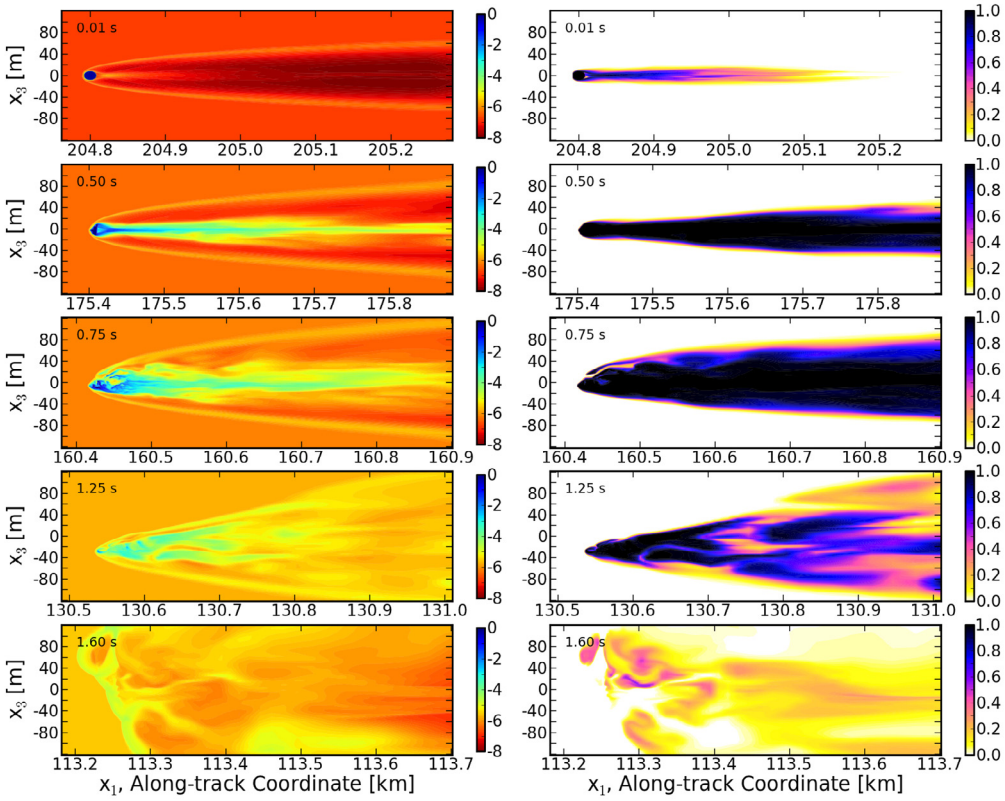

Fig. 9. Progression of the 2012 impactor's disintegration during its descent into the Jovian atmosphere in the $x_2 = 0$ plane. Plotted variables are logarithm of density (*left column*) in units of $\log_{10}$ (g cm^{-3}) and mass fraction of comet material vs. Jovian air (*right column*) in units of $g_{H_2O}\, g_{air}^{-1}$.

of the debris. The aerodynamic loading on the large fragments breaks them into smaller but rather coherent parts, while it shreds the smaller cometary debris into a cloud of material that quickly decelerates and transfers its kinetic energy to the atmosphere. The impactor undergoes multiple fragmentation events, and the last major one occurs at $z \approx 100$ km altitude. After this event, the remaining material travels farther into the atmosphere by its momentum. At $t \sim 2.25$ s, the material stops and reaches its terminal depth at $z = 81$ km, corresponding to the 16 hPa pressure level.

The distribution of debris is similar to what is generated by an SL9 (Palotai et al. 2011) or 2009-type impactor (Pond et al. 2012). To track where the comet material is deposited in the atmosphere during the entry phase, we calculate the mass loss of the impactor throughout its descent (Fig. 11). Initially, the debris material is restricted to a narrow streak behind the impactor that is constrained by the shock wave structure in that region (Fig. 9, top right panel). This results in a mass loss of only a few percent before the object breaks up at $z \approx 120$ km altitude. Below this level there is a rapid increase in mass loss, and the rate at which the leading major fragment loses material is nearly constant down to $z \approx 100$ km. This rate is about 6.1% of the initial mass of the object or 78.4 Tn per kilometer. At the final stage of the impact, there is only a small amount of coherent material, which completely disintegrates and stops at the terminal depth.

Figure 12 presents the temperature field around the impactor and in its wake during the atmospheric entry. Temperatures behind the impactor are up to about 10 000 K, and they can be as high as 40 000 K between the rear shock and the turbulent wake. There are higher temperatures in front of the impactor; for instance, the stagnation point temperature before the main breakup event is above 100 000 K. This temperature is higher than previously calculated values by Boslough et al. (1995) and Crawford (1996). At 0.6 s in our simulation (Fig. 12), the sound speed at the impactor's altitude is 897 m s^{-1} and the resulting Mach number is $M = 66.9$. Our model output temperature values are consistent with estimates from gas dynamical calculations of the stagnation point temperature behind the bow shock at this Mach number (Anderson 2002). The model uses ideal gas to calculate these temperatures, so our values are overestimates by not accounting for the ionization and dissociation of the gas. After the fragmentation events, both the bow shock and the rear shock that generate the high temperatures collapse, and at that point the highest temperature values reach about 10 000 K.

6. Flux rate of impacts in Jupiter

It is difficult to judge the significance of three bolide flashes serendipitously observed by an uncoordinated network of amateur astronomers. The discovery of the first Jupiter bolide in June 2010 was so unexpected that previous observations of bolides may have been misinterpreted as cosmic rays or atmospheric phenomena on Earth. Therefore, statistics of small Jupiter impacts have only been possible since the first unambiguous discovery of a small impact. The Planetary Virtual Observatory and Laboratory (PVOL, Hueso et al. 2010a) is the database of images of the International Outer Planets Watch (IOPW) contributed by more than 250 amateur astronomers worldwide. Figure 13 shows the number of Jupiter observations per week available in this database since January 2010. Each file may contain several observations from the same night, each one acquired by filming the planet with a CCD video camera. Each observation in the database is equivalent to a video film of the planet of three to five minutes on average, and since several

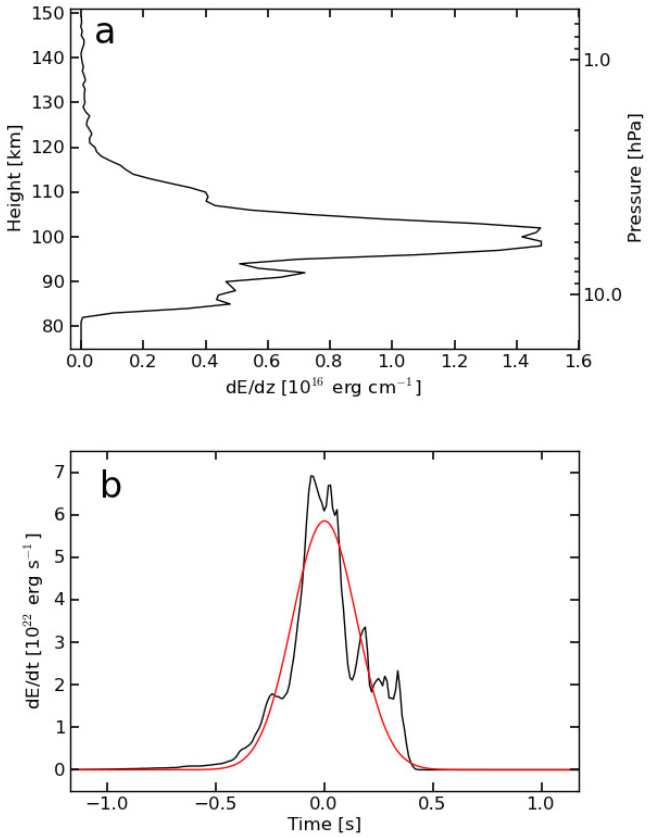

Fig. 10. Energy-deposition profile of a 16-m diameter ice impactor entering Jupiter's atmosphere in terms of atmospheric height **a)** and time **b)**. The rapid increase in the deposited energy at 120 km indicates the initial breakup of the object, and the sharp peak at about 100 km altitude represents the disintegration of the last big coherent fragment. The time behavior of energy release compares well with the light curves analyzed in the three impacts. Significant structure in the synthetic light curve is found in time scales of 0.05 s, suggesting an ideal time-resolving observation of 20 frames per second. A Gaussian fit to the energy release in terms of time appears in panel **b)**. The FWHM of this fit is 0.35 s. The bright explosion is followed by further release of energy when the rests of the impacting object desintegrate 90 km above the 1 bar level. This behavior seems similar to the one present in the light curves from the June 2010 and August 2012 impacts.

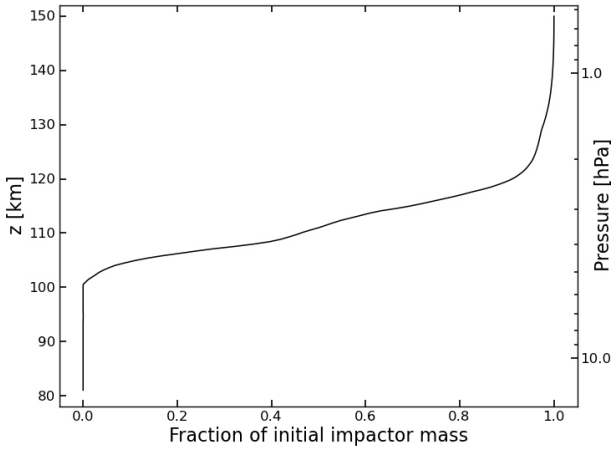

Fig. 11. Mass loss of the Jovian impactor in our simulation in terms of the object's initial mass, 1287 Tn. After the initial breakup of the object at about 120 km altitude, the rate at which debris is shredding off of the impactor is nearly constant with a value of 78.4 Tn km^{-1}.

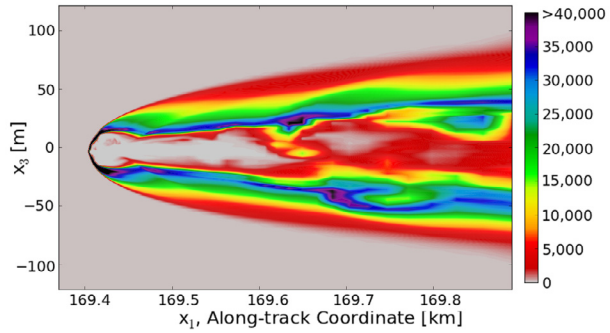

Fig. 12. Temperature field in the vicinity of the impactor at 0.6 s into the simulation in the $x_2 = 0$ plane. Units are K.

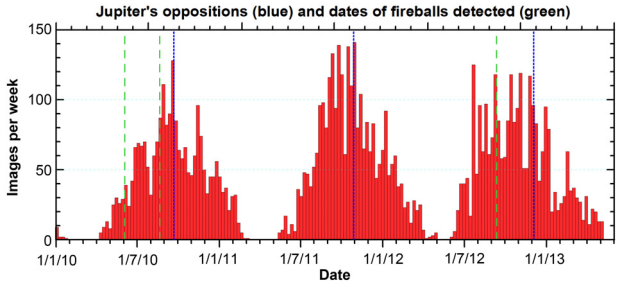

Fig. 13. Number of Jupiter observations per week in the PVOL server over the past 3 years. Vertical dashed lines correspond to the dates of the three impacts. Dotted vertical bars correspond to Jupiter oppositions. The irregular cover of the latest Jupiter apparition corresponds to bad weather conditions over winter 2012–2013. The total number of images in this period is 7984.

images are available in many image registries each registry in the database is roughly equivalent to ten minutes of observations. Additionally, each image represents only the best observations in a longer series, and the total observation times from one observer obtaining and submitting an image to the database may grow to 30 min. The database contains 8000 images from January 2010 to April 2013 adding up to 170 days of observation accumulated over three years and four months, which would represent 13% of the total possible time. A still larger database of amateur images of Jupiter is that of the Association of Lunar and Planetary Observers in Japan (ALPO Japan, see http://alpo-j.asahikawa-med.ac.jp/indexE.htm) with more images from Asian observers. However, both databases are incomplete, as is demonstrated by the fact that two of the three fireballs were discovered by irregular contributors to any of them. Additionally, only a fraction of amateur observers examine their video observations of the planet closely enough to spot small impacts. This is exemplified by the fact that the three impacts were first detected by one observer and then later found by a second observer in his data. In summary, the total effective time Jupiter is observed over a year might be estimated as 10–30% but the detection efficiency of bolides in recorded videos is probably lower than 50%.

The geographical distribution of amateur observers worldwide peaks in Europe, Japan, North America, and Australia (Hueso et al. 2010a), and most observations are clustered on days where good weather is prevalent in these geographical areas. The upper bound of 30% for the effective observing time is close to an estimation coming from the geographical distribution of observers when assuming Jupiter is always observed by someone in Japan/Australia, Europe, and North/South America when the planet is high enough in the sky and considering that only six months of frequent observations are possible each year

around Jupiter opposition. If we take weather conditions into account, this number may be lowered to 20%.

If we assume an effective observation time fraction of 10−30% for the global community of amateur observers, and we consider that three impacts have been detected in roughly 35 months (from June 2010 to April 2013), and if we furthermore consider a detection efficiency of 30−50%, this extrapolates to 6−30 "potentially detectable" impacts per year. We do not consider times previous to June 2010 because we assume that any impact would not have been clearly identified by the observer.

Additional arguments that help constrain the number of impacts come from the observations of a single dedicated observer closely examining his own video observations for impact detections. A.W. observed Jupiter in 2010 during 52 h accumulated over one year in different observational runs. This is about 0.6% of the total possible time per year. In four years A.W. has observed a large impact (Sánchez-Lavega et al. 2010) and a single flash. If this single impact is extrapolated to the total number of impacts in three years, this is equivalent to a flux rate of "detectable impacts" of 160 per year. This number represents an absolute upper bound to the flux rate since the statistics are biased by the positive single event detection. Similar numbers are extracted from observations performed by C.G. (roughly 120 h of observations accumulated since June 2010). The other observers that have successfully detected impacts in Jupiter do not observe the planet intensively enough to extract a significant conclusion from their observations, and there are other highly qualified observers with similar observing routines that have not detected any impact. A better argument about the flux rate of objects into Jupiter comes from a collaboration between amateurs closely examining video observations of Jupiter with a software designed specifically for that purpose (see Sect. 7). This has resulted in a negative detection after close examination of 7826 video observations for a total accumulated time of 6.1 days extending from 2006 to 2013. From this negative result, the total rate of "detectable impacts" should be lower than 60 objects per year, compatible with the ranges given above.

Since ground-based observations of Jupiter can only survey a fraction of the planet's area (the day side of the planet excluding the polar regions) the number of detectable impacts would correspond to a rate of impacts in Jupiter that is two times higher, which is equivalent to 12−60 objects of 5−20 m size impacting Jupiter every year.

7. Impact detection

There are two main areas where work is needed to reduce the uncertainty in the flux rate of impacts on Jupiter. First, a coordinated observation campaign aimed at attaining a large accumulated time of observations may discover more objects and may be statistically significant after a large accumulated time close to opposition. As determined above, the estimated flux rate of detectable objects is in the range of 0.07% to 0.35% per observation hour. If the impact rate is high, six days of accumulated observations would be needed to have a 50% probability of detecting one object. However, if the impact rate is low, 30 days of accumulated observations would be required to have a 50% probability of detecting one object. In both scenarios, a strong effort is required to purposely detect an impact. Such a mission cannot be undertaken by a single research group unless a robotic telescope with an automatic acquisition and analysis software is devoted to the task. An alternative solution consists of using a relatively large telescope (50 cm aperture or more) able to detect more frequent, less massive impacts with sizes of 3−5 m.

Whether a robotic telescope is dedicated to this job or a coordinated collaboration between several observers is initiated, ideal observations intended to detect and characterize future impacts could benefit from observation runs with a low frequency of 10−15 fps. This is enough to recover light-curve characteristics and is more sensitive to the tail of the light curve, as well as to smaller, fainter objects. Filters where the planet is dark but a fireball radiating at 4000−10 000 K is bright may be useful. An ideal system consisting of two telescopes equipped with a blue and methane filter would detect the impacts and constrain their brightness temperatures and energies. Simulations of impacts show that high temperatures are produced, and it is not inconceivable that immediate Earth-based observations could detect the thermal shock signature of a small impactor, although this point deserves further research.

On the other hand, thousands of hours of Jupiter observations are already available in the observations acquired by the global network of amateur astronomers. The analysis of this amount of data requires automatic analysis tools able to detect faint impacts in the recorded videos. Together with amateur astronomers, we have developed two software tools able to detect impacts on Jupiter from video observations. Detection algorithms are based on coregistering the individual frames and obtaining difference images with a reference image built from the video, essentially working similarly to the software described above to automatically extract light curves. Both pieces of software can analyze videos generated by cameras used by amateur astronomers written with video codecs such as the black and white uncompressed AVI Y800 codec and the SER format. Both software programs can work in batch mode and produce lists of impact flash candidates. One of them is JID (Jovian Impact Detector) which is suitable for Windows users and can also work in Linux and MacOS. The software incorporates an easy to use intuitive Graphic User Interface.

The other package, DeTeCt: Jovian Impact DeTeCtion Software, also works in Windows and Linux but in batch-command mode. It additionally generates differential images between maximum brightness images and mean images of an overall video (see Fig. 5, panel d) that can be useful for quick visual inspection and log files with observation times useful for statistical analysis. This package is being used in a growing amateur project by about 20 amateur astronomers (mainly from France). The resulting analysis of almost 8000 videos has provided negative detection placing the upper limit on impacts in Jupiter of 60 per year quoted in the previous section. Details are given in the project webpage, http://www.pvol.ehu.es/software/, and in the statistical analysis developed on http://www.astrosurf.com/planetessaf/doc/project_detect.shtml

8. Conclusions

Regular continuous monitoring of Jupiter by the broad community of amateur astronomers and advances in low-cost astronomical cameras have resulted in the discovery of three small impacts in the planet. The one-to three-second duration of these Jovian flashes is similar to the duration of intense flashes caused by explosions of bolides observed on Earth caused by objects 1−10 m in size, which release energies of 20−100 kTn (Brown et al. 2002; Jenniskens et al. 2009). In the case of the Jovian fireballs, differences in the durations of each bolide might not be real but are introduced by systematic differences between

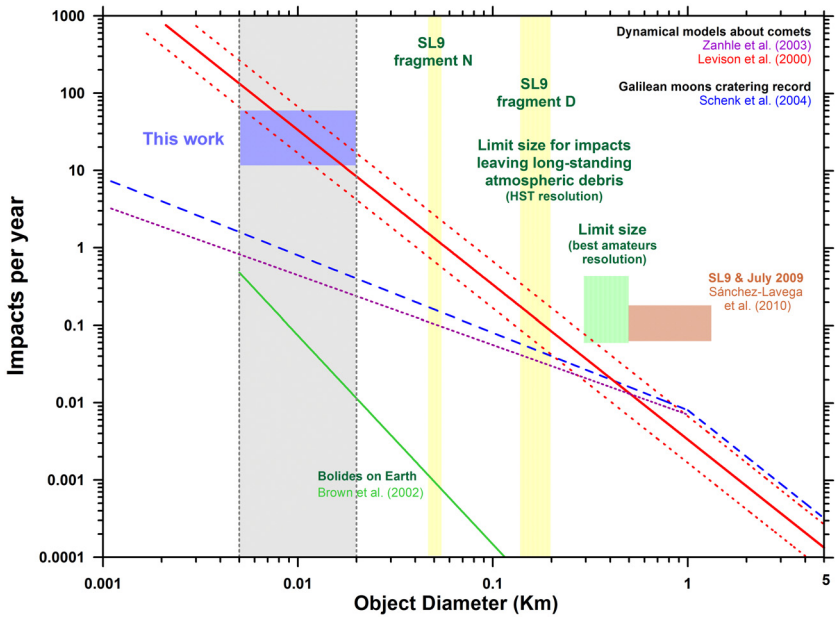

Fig. 14. Impact rates on Jupiter and Earth compared. Vertical gray regions represent the sizes of the three bolides discussed in this work. The blue box represents the impact rate of 5−20 m size objects in Jupiter. Lines represent impact rates from dynamical models of comets (red line with estimated uncertainties in dotted line, Levison et al. 2000) or the cratering record in Galilean moons (blue line, Schenck et al. 2004). The yellow regions indicate limiting size of objects that could be discovered by the dark debris they should leave in Jupiter's atmosphere. The small SL9 N fragment would only be observable for a few planetary rotations at the resolution attainable with the HST. A long-standing debris feature is probably associated to objects of 200 m in size such as SL9 fragment D. The light-brown box represents estimates of impact rates on Jupiter from Sánchez-Lavega et al. (2010) for 0.5−1 km size objects. The green box represents objects leaving debris field that could be detected with amateur equipment.

Table 5. Summary of impacts on Jupiter.

Date (yr-mm-dd)	Mass	Size	Reference
1981-03-05	11 kg	44 cm	Cook & Duxbury (1981)
1994-07-16 to 1994-07-24	1.0×10^9 Tn	2 km	Hammel et al. (1995) Harrington et al. (2004)
2008-07-19	6.0×10^7 Tn	0.5 km	Sánchez-Lavega et al. (2010) Hammel et al. (2010)
2010-06-03	105−780 Tn	5−18 m	Hueso et al. (2010b), this work
2010-08-20	205−610 Tn	6−17 m	This work
2012-09-10	500−950 Tn	8−19 m	This work

the observations. The bright flashes analyzed here lie in the range of masses between the 2009 June impact (Sánchez-Lavega et al. 2010), which had a mass that is 10^5 higher and which produced strong atmospheric effects observable for months (Hammel et al. 2010), and the small fireball observed by Voyager 1 in 1981, which is 10^5 times less massive (Cook & Duxbury 1981).

The main characteristics of Jupiter impacts are summarized in Table 5. Densities are assumed to be 0.25 g/cm^3 for the SL9 (icy porous body) and 1981 small fireball and 1.0 g/cm^3 for the 2009 impact with a debated asteroidal nature. The deep gravitational well of Jupiter accelerates these objects to collision speeds of 60−70 km s^{-1}, making collisions 10−40 times more energetic than equivalent objects colliding with the Earth. An extrapolation of the expected impact rate in the Jovian system from the cratering record in Galilean satellites (Schenk et al. 2004; Zahnle et al. 2003) would predict one impact of a 10 m size object per year on Jupiter, but an extrapolation of the dynamical models of comets and asteroids in orbits prone to Jupiter encounters (Levison et al. 2000) produces an expectation of 30 to 100 such collisions every year. The latter estimate is close to the values we computed in this paper (12−45) from the current observations. Figure 14 summarizes the expected impact rates from the cratering record, dynamical models and the observations discussed in this paper.

To better constrain the values in this figure, more observations of impacts are needed, as well as the statistics of the observations required to find more impacts. Detecting 10 m size objects colliding with Jupiter is achievable with amateur equipment, but smaller objects with sizes on the order of 5 m may collide with Jupiter ten times more frequently, indicating that detection campaigns with larger telescopes than those available to amateurs can significantly enhance the detection rate. On the other hand, larger objects like the 7.5−20 m size object colliding with Jupiter on September 2012 should also be detectable on Saturn with amateur equipment. The largest impactor detected in Saturn rings from *Cassini* observations of ejecta clouds had an estimated size of 2−20 m in diameter (Tiscareno et al. 2013). Such objects can produce detectable flashes on amateur equipment when impacting the planet. Additionally, from the estimated collision rate of small objects, large objects of 200 m in diameter releasing 10 000 times more energy than the June 2010 Jovian bolide may collide with Jupiter once every couple of years, and be detectable for a few weeks through images of unusual dark features on the planet, allowing the possibility

of discovering such intermediate size objects (between the 2009 impact and the 2012 superbolide) about once or twice a decade.

Our model draws a physically self-consistent picture of the impact circumstances that is consistent with the time scales of the observed fireballs. The agreement should be considered as approximate in light of the many uncertainties, which include the real size, mass, density, and impacting angle, as well as observational uncertainties on the light curves themselves. The model suggests that atmospheric perturbations by the impactor are limited to pressures lower than 16 hPa. Owing to computational constraints, we could not include a larger domain to properly investigate the plume genesis in the wake of the impactor, but it is unlikely that impactors similar to the 2010 and 2012 objects generate a debris field that can be observed from Earth. However, the simulations suggest that the thermal shock signature of a small impactor could be detected from Earth-based telescopes in immediate observations after a small impact.

The flux of impacts on Jupiter gives information about the population of small objects impacting the planet. By constraining the impact rate, we can get insight into the history of delivery of minor chemical species to the giant planet and stratospheric chemistry (Cavalié et al. 2013). Additionally, if we compare the estimated flux of impacts on Jupiter with the rate of impacts observed on Earth, we observe a Jovian flux of impacts that is a few hundred times larger than on Earth. Although the objects impacting Jupiter and the Earth have very different populations and dynamical histories, the scaling factor roughly corresponds to the larger cross section of Jupiter (120 larger than the Earth's) and gravitational potential (315 greater than the Earth's) diminished by the larger volume of space occupied by its orbit. The high flux of impacts offers opportunities for understanding the atmospheric consequences of large airbursts like those of Tunguska or Chelyabinsk. While these events happen on Earth on time scales of a century or more, they happen on Jupiter on time scales of a week to a few months.

Acknowledgements. This work was supported by the Spanish MICIIN projects AYA2009-10701 and AYA2012-36666 with FEDER funds, by Grupos Gobierno Vasco IT765-13 and by Universidad País Vasco UPV/EHU through program UFI11/55. It was also supported by National Science Foundation grant AST-1109729 and NASA Planetary Atmospheres Program grant NNX11AD87G. This work is partially based on observations from the following telescopes. (1) HST (program GO/DD-12119), with support provided by NASA through a grant from the Space Telescope Science Institute, which is operated by the Association of Universities for Research in Astronomy, Inc. under NASA contract NAS 5-26555. (2) TRECS and NIRI at the Gemini Observatory (program GS-2010A-DD-64 and GN-2010A-DD-4), which is operated by the Association of Universities for Research in Astronomy, Inc., under agreement with the NSF on behalf of the Gemini partnership: the National Science Foundation (United States), the Science and Technology Facilities Council (United Kingdom), the National Research Council (Canada), CONICYT (Chile), the Australian Research Council (Australia), Ministério da Ciência e Tecnologia (Brazil) and Ministerio de Ciencia, Tecnología e Innovación Productiva (Argentina). (3) VLT/VISIR (program 60.A-9800(I)) at the European Organization for Astronomical Research in the Southern Hemisphere, Chile. (4) NIRC2 at the W. M. Keck Observatory, which is operated as a scientific partnership among the California Institute of Technology, the University of California, and the National Aeronautics and Space Administration. The Observatory was made possible by the generous financial support of the W. M. Keck Foundation. (5) TEXES at the Infrared Telescope Facility, which is operated by the University of Hawaii under Cooperative Agreement NNX-08AE38A with the National Aeronautics and Space Administration, Science Mission Directorate, Planetary Astronomy Program.

References

Anderson, J. D. 2002, Modern compressible flow: with historical perspective, 3rd edn. (McGraw-Hill)
Baines, K. H., Yanamandra-Fisher, P. A., Momary, T. W., et al. 2013, Planet. Space Sci., 77, 25
Bell, J. F., Squyres, S. W., Arvidson, R. E., et al. 2004, Science, 305, 800
Borovička, J., & Charvát, Z. 2009, A&A, 507, 1015
Boslough, M. B. E., & Crawford, D. A. 2008, Int. J. Impact Eng., 35, 1441
Boslough, M. B., Crawford, D. A., Trucano, T. G., & Robinson, A. C. 1995, Geophys. Res. Lett., 22, 1821
Brown, P. 2013, IAA Planetary Defense Conference, Flagstaff, Arizona, April 2013
Brown, P., Spalding, R. E., ReVelle, D. O., Tagliaferri, E., & Worden, S. P. 2002, Nature, 420, 294
Byrne, S., Dundas, C. M., Kennedy, M. R., et al. 2009, Science, 325, 1674
Cavalié, T., Feuchtgruber, H., Lellouch, E., et al. 2013, A&A, 553, A21
Ceplecha, Z., Spalding, E. R., Jacobs, C., et al. 1999, in Meteroids 1998, eds. W. J. Baggaley, & V. Porubcan, 37
Chanover, N. J., Kuehn, D. M., Banfield, D., et al. 1996, Icarus, 121, 351
Chapman, C. R. 1996, in IAU Colloq. 156, The collision of comet Shoemaker-Levy 9 and Jupiter, eds. K. S. Noll, H. A. Weaver, & P. D. Feldman, (Cambridge University Press), 121
Cook, A. F., & Duxbury, T. C. 1981, J. Geophys. Res., 86, 8815
Crawford, D. A. 1996, in The collision of comet Shoemaker-Levy 9 and Jupiter, IAU Colloq. 156, eds. K. S. Noll, H. A. Weaver, & P. D. Feldman (Cambridge: Cambridge University Press), 133
Crawford, D. A. 1997, Ann. New York Acad. Sci., 822, 155
Daubar, I. J., McEwen, A. S., Byrne, S., Kennedy, M. R., & Ivanov, B. 2013, Icarus, 225, 506
de Pater, I., Fletcher, L. N., Pérez-Hoyos, S., et al. 2010, Icarus, 210, 722
de Pater, I., Wong, M. H., de Kleer, K., et al. 2011, Icarus, 213, 559
Deming, D., & Harrington, J. 2001, ApJ, 561, 468
Fletcher, L. N., Orton, G. S., de Pater, I., & Mousis, O. 2010, A&A, 524, A46
Fletcher, L. N., Orton, G. S., de Pater, I., et al. 2011, Icarus, 211, 568
Hammel, H. B., Beebe, R. F., Ingersoll, A. P., et al. 1995, Science, 267, 1288
Hammel, H. B., Wong, M. H., Clarke, J. T., et al. 2010, ApJ, 715, L150
Harrington, J., de Pater, I., Brecht, S. H., et al. 2004, in Jupiter: the planet, satellites and magnetospheres, eds. F. Bagenal, T. E. Dowling, & W. B. McKinnon (Cambridge, UK: CUP), 159
Hayes, J. C., Norman, M. L., Fiedler, R. A., et al. 2006, ApJS, 165, 188
Horner, J., & Jones, B. W. 2008, Int. J. Astrobiol., 7, 251
Horner, J., & Jones, B. W. 2009, Int. J. Astrobiol., 8, 75
Horner, J., & Jones, B. W. 2012, Int. J. Astrobiol., 11, 147
Horner, J., Jones, B. W., & Chambers, J. 2010, Int. J. Astrobiol., 9, 1
Hueso, R., Legarreta, J., Pérez-Hoyos, S., et al. 2010a, Planet. Space Sci., 58, 1152
Hueso, R., Wesley, A., Go, C., et al. 2010b, ApJ, 721, L129
Huestis, D. L., & Slanger, T. G. 1993, J. Geophys. Res., 98, 10839
Jenniskens, P., Shaddad, M. H., Numan, D., et al. 2009, Nature, 458, 485
Karkoschka, E. 1998, Icarus, 133, 134
Korycansky, D. G., Harrington, J., Deming, D., & Kulick, M. E. 2006, ApJ, 646, 642
Levison, H. F., Duncan, M. J., Zahnle, K., Holman, M., & Dones, L. 2000, Icarus, 143, 415
Malin, M. C., Edgett, K. S., Posiolova, L. V., McColley, S. M., & Dobrea, E. Z. N. 2006, Science, 314, 1573
Melosh, H. J. 1989, Impact cratering: a geologic process (New York: OUP)
Noll, K. S., Weaver, H. A., & Feldman, P. D. 1996, The collision of comet Shoemaker-Levy 9 and Jupiter, Space Telesc. Sci. Inst. Symp. Ser., 9
Ortiz, J. L., Sada, P. V., Bellot Rubio, L. R., et al. 2000, Nature, 405, 921
Ortiz, J. L., Aceituno, F. J., Quesada, J. A., et al. 2006, Icarus, 184, 319
Orton, G. S., Fletcher, L. N., Lisse, C. M., et al. 2011, Icarus, 211, 587
Palotai, C., Korycansky, D. G., Harrington, J., Rebeli, N., & Gabriel, T. 2011, ApJ, 731, 3
Pérez-Hoyos, S., Sanz-Requena, J. F., Sánchez-Lavega, A., et al. 2012, Icarus, 221, 1061
Pond, J. W. T., Palotai, C., Gabriel, T., et al. 2012, ApJ, 745, 113
Sánchez-Lavega, A., Wesley, A., Orton, G., et al. 2010, ApJ, 715, L155
Sánchez-Lavega, A., Orton, G. S., Hueso, R., et al. 2011, Icarus, 214, 462
Sánchez-Lavega, A., Rojas, J. F., Hueso, R., et al. 2012, Proc. SPIE, 8446, 7
Schenk, P. M., Chapman, C. R., Zahnle, K., & Moore, J. M. 2004, in Jupiter: the planet, satellites and magnetospheres, eds. F. Bagenal, T. E. Dowling, & W. B. McKinnon (Cambridge, UK: CUP), 427
Selsis, F., Lemmon, M. T., Vaubaillon, J., & Bell, J. F. 2005, Nature, 435, 581
Tabe, I., Watanabe, J.-I., & Jimbo, M. 1997, PASJ, 49, L1
Tillotson, J. H. 1962, in General Atomic Report GA-3216 (San Diego, CA: General Atomic)
Tiscareno, M. S., Mitchell, C. J., Murray, C. D., et al. 2013, Science, 340, 460
Watanabe, J., Tabe, I., Sugita, S., et al. 2012, LPI Contributions, 1667, 6271
Wetherill, G. W. 1994, Ap&SS, 212, 23
Zahnle, K., Schenk, P., Levison, H., & Dones, L. 2003, Icarus, 163, 263